Modelling the reaction of uranium with carboxylic groups on surfaces through mono- and multi- dentate surface complexes on the basis of pH and redox potential

Steven McGowan, Claude Degueldre*, Farid Aiouache

Engineering Department, Lancaster University, Lancaster LA1 4YW, UK

ARTICLE INFO

ABSTRACT

An analytical expression is proposed to simulate effects of pH and redox potential (E) on the sorption of uranium onto bioorganic model particles in saline or other aquatic environments. The elaborated expression is intended to avoid use of the classical approach of sorption which relies on experimental data and empirical models. The goal is to produce an expression that provides a distribution coefficient (Kd e.g. mL g^{-1}) as function of pH, E and ligand concentration (through complex formation in solution) by applying a surface complexation model on one type of mono-dentate surface sites > (SuOH) as well as utilizing multi-dentate surface sites > (SuOH)$_c$. The formulation of the worked out expression makes use of correlations between the surface complexation and hydrolysis constants for all species and sorption sites. The model was applied to the sorption of uranium onto bioorganic sites with and without carbonates in solution e.g. Log Kd: + 2.75 at pH 8 for 2 sites per nm^2. The calculated distribution coefficients were found very sensitive to the presence of carbonates, e.g. Log Kd: − 7.0 at pH 8 for 2×10^{-3} M total carbonate. The potential reduction of uranium U(VI) and its complexes (carbonates) which are the primary stable species in surface waters, to U(IV) during sorption was simulated in association with a decrease in the redox potential and was found generally below the redox stability limits of water. The calculated distribution coefficient values were validated by the values reported in literature for the sorption of uranium onto specific adsorbents. The investigated simulations are also applicable to the sorption of other redox sensitive elements.

1. Introduction

While the fuel cycles are under constant review in terms of efficiency and safety, the relevant economic aspect remains dictate the preferred route towards the geological source of uranium (U) for the operation of current nuclear systems, see Ewing [1].

A potential alternative to geological solid ore sources would be extraction of uranium from seawater e.g. Degueldre [2] or Tsouris [3]. It is present at concentration of trace scale with an average of 3.3 parts per billion (ppb) in standard seawater conditions (i.e. 35% salinity and pH 8.0). This uranium is present in multiple forms, including (in order of prevalence) tricarbonato-uranyl [$UO_2(CO_3)_3^{4-}$], dicarbonato-uranyl [$UO_2(CO_3)_2^{2-}$], uranyl tri-hydroxide [$UO_2(OH)_3^-$], uranyl [UO_2^{2-}], uranyl hydroxide [$UO_2(OH)^+$], and uranyl di-hydroxide [$UO_2(OH)_2$]. The dominant form (84.9%), the tricarbonato-uranyl, is most commonly assumed to be bound to calcium ion as reported by Djogic &

Branica [4], Zhang et al. [5], Sekiguchi et al. [6], Aihara et al. [7] and Yamashita et al. [8].

There have been attempts to extract uranium resource on test scales. The most successful one was run by Sugo et al. [9], who placed braided chains of amidoxime-grafted polyethylene in deep-water conditions. This is considered the "Best Possible Technology" existing so far for the application but remains uneconomic under current market conditions e.g. Sugo et al. [9]; Schneider & Sachde [10] and NEA & IAEA [11].

A potential alternative to this approach would be the use of a natural material to sorb uranium which would not require specific absorbent synthesis. Many natural materials include structures that are anticipated to interact selectively with relevant elements in solution. These can be the functional, nutritional or protective parts of the biological structure. However, the original purpose is actually irrelevant, if the relevant compounds can be straightforwardly extracted, as suggested by Gaur et al. [12].

* Corresponding author.
E-mail address: c.degueldre@lancaster.ac.uk (C. Degueldre).

The materials specifically tested with uranium included *Myricae Cortex* barks (Nakajima & Sakaguchi [13]), *Citrus limetta* peels (Gondhalekar & Shukla [23]), pyrolyzed tea and coffee wastes (Aly & Luca [14]) and *Citrus* reprocessing wastes (Satari & Karimi [26]; Pathak et al. [15]). Recently the sorption of uranium from seawater was tested on several biomaterials by McGowan et al. [16]. On the other side several transition metal sorption on polycarboxylic loaded microspheres were tested in seawater conditions by Dakova et al. [17].

These miscellaneous organic molecules, referred also "biomass", are complex and of unpredictable structures. By capacity, the most common binding sites in plant biomass are carboxylic, with other structures considered in future works. These structures serve a variety of functions in biological processes and offer consistent binding capacity over the pH range that the biomaterial may meet, as reported by Vaz [18].

Sorption behaviour is generally characterised by the sorption isotherms. These can range from a Langmuir isotherm, see Langmuir [19], on strong interacting sites at low concentration to a Freundlich [20] isotherm on weak site at higher concentrations. When all strong sites are saturated, either as single groups or multi-sites, e.g. Padilla et al. [21], the sorption will experience association on weaker sires, followed by sorption saturation or surface precipitation at higher concentrations, as reported by McKinley & Scholtis [22].

From a mechanism point of view the sorption reactions on hydrophilic objects may be described by the following specific processes. In low pH, on strong acid sites, ion exchanges drive the sorption processes, typically on single sites, see Millar et al. [23], and Millar et al. [24], but it can also occur on multi-sites, see Wissocq et al. [25] and in an ambiguous way, see Reinoso-Maset & Ly [26]. At higher pH and weak ionic strength, on weak acid sites, the driving sorption mechanism becomes surface complexation, e.g. Esfandiar *et al* [27]. When hydrophobic interactions take place specific sorption enhancement may be observed e.g. Cai et al. [28].

All sorption mechanisms can be affected by variations of the system equilibria, including competition between the free ions of various elements, complexes (with ligands in fluid and solid phases) and their redox states. For examples surface complexation can be affected by pH effects, by complexation competitions in the aqueous phase, e.g. Mei et al. [29] and/or at the surface, e.g. Burdzy et al. [30], as well as by oxydo-reduction reactions, and as a combination of these reactions, see Alonso & Degueldre [31]. Surface precipitation may also complete these reactions at higher concentration as reported by Degueldre & Kline [32]. Aside from these well documented processes, the sorption of a particular metal ion M_1 can also be affected by the competition with the sorption of metal ion M_2, e.g. Padilla et al. [33]. These reactions may be simulated via thermodynamic models as reported by Missana et al. [34].

In regard of the materials of interest, in addition to these direct binding processes, biomass also includes many chemical structures intended to control the redox potential, which has important implications for the capture processes, such as reduction of mobile forms of the uranium to immobile ones in situ, and through release into solution. This increasing binding effect serves to accelerate capture, reducing release, see Lovley et al. [35] and Senko et al. [36]. Furthermore, the biomaterials often include nutritional benefits for microorganisms, which further boost these deposition processes such as those detailed by Senko et al. [36].

Here, the materials of interest are by-products, or otherwise low cost biomaterials, which can be dried effectively, with high surface area including antioxidant compounds as suggested by Degueldre et al. [37]. This study is part of an attempt to develop an alternative nuclear fuel cycle, including uranium extraction from seawater, and its utilization in a fast molten salt reactor, in order to develop a renewable nuclear fuel cycle as described recently in Degueldre et al. [37].

The objective of this study is to simulate, by a systematic methodology, the extraction mechanism on a model biomaterial loaded with

carboxylic groups. Our proposed model is applied in a comprehensive way to simulate the sorption of uranium onto these organic particles considering the effects of pH, E, ligand concentrations in the aqueous phase. Here, the specific site structures of adsorbents (e.g. mono-, bi-, tri- dentate complexes) have been used to selectively sorb the element of interest. The methodology is aimed to evaluate the surface complexation constants of all involved species by correlations, as reported earlier for mono-dentate surface complexes, and to apply this methodology for multi-dentate surface complexes to achieve the sorption study in a more complete way.

The effect of redox potential on the simulation of uranium sorption onto inorganic particles has already been reported by Degueldre & McGowan [38]; the present study investigates for the first time simulations of uranium sorption onto organic particles covered with carboxylic active groups. In the following two sections, the modelling of species occurrence and their sorption properties is presented and calculated for the liquid and the sorbent phases within environmental contexts.

2. Modelling species occurrence and their sorption properties

The sorption process of metal species is a consequence of a complex series of reactions. These include the formation, alteration or deconstruction of complexes with ligand in solution or with active surface sites of "weak acid" nature (somewhat covalent bound). When occurring on surfaces, it is referred to a surface complexation, as a distinction from ion exchange processes with the "strong acid" active sites (ionic bound). It is best described by the distribution ratio (R_d), which yields a distribution coefficient (K_d) in mL g^{-1} at the sorption/desorption equilibrium:

$$K_d = \frac{[M]_{sorb}}{[M]_{sol}} \tag{1}$$

W Where $[M]_{sorb}$ and $[M]_{sol}$ are the total concentrations of the element sorbed on the particles (in mol g^{-1}) and present in solution (mol mL^{-1}), respectively.

In the context of low density compounds, such as the organic materials, it is often difficult to measure the concentration $[M]_{sorb}$ at the surface of the particulate material at equilibrium, so it is necessary to modify Eq. 1 to include the particle concentration as an additional factor and adapt it to wet phase conditions. K_d becomes:

$$K_d = \frac{[M]'_{sorb}}{[M]'_{sol}} \frac{1}{[Part]} \tag{2}$$

Where both (total) concentrations $[M]'_{sorb}$ and $[M]'_{sol}$ are given in mol mL^{-1} and [part] is the particle concentration in g mL^{-1}.

2.1. Site availability

For the purpose of this implementation in the model, the surface was considered to be a spherical particle of fixed average size, defined by radius r in nm. From this, the average surface area (S) can be calculated using Eq. 3. With addition of the material specific mass in g nm^{-3}, the average mass (m_a) can be calculated as per Eq. 4.

$$S = 4 \pi r^2 \tag{3}$$

$$m_a = (4/3) \pi r^3 \tag{4}$$

S is calculated in nm^2 and m_a is derived in g.

For the purposes of standardising the structure, the plane was supposed to be rectangular, of dimensions *a* and *b* with *c* sites interacting with the ion or the available complex. This shape was selected to allow easy use of unit cell dimensions from crystallisation studies, for example as gained from Jones & Templeton [39]. Note that non-interactive materials, such as unsuitable molecule orientations, hydrating

water molecules, or underlying mounting matrix average the molecular site surface density c/ab in mol nm^{-2} can be combined with S to estimate an average amount of site (mol) per particle.

In previous implementations of this model, such as Degueldre & McGowan [38], the surface site density was taken directly from empirical (experimental) results. Calculations based on fixed physical characteristics allowed this value to be intrinsically justified.

Consequently, the site molar density N_s (mol per average particle surface area) was estimated using the average surface area of the particle as calculated in Eq. 3, and the total surface, as displayed in Eq. 5:

$$N_s = cSN_{av}^{-1} (1 - I) a^{-1}b^{-1} \tag{5}$$

where c being active sites number at the surface $(a \cdot b)$, I the inactive surface fraction and N_{av} being Avogado's constant.

Total site concentration $([> Su]_{tot})$ in mol mL^{-1} was then calculated from the site density, average mass and the particle concentration [part]:

$$[>Su]_{tot} = \frac{N_s. \, [\text{part}]}{m_a} \tag{6}$$

The $[> Su]_{tot}/[\text{part}]$ ratio may be estimated experimentally using the specific surface provided by BET measurements, which was used to verify the results. Note that the site can be formulated as $> Su, > SuOH, > SuO^-, > (SuOH)_c, \ldots$ according to conditions.

2.2. Effect of acidity on the sites

The most common protonated form of site is $> (SuOH)_c$. As the sites which are suitable to be receptive to the metal ion can be modified by protonation and deprotonation of the sites at different pH's. These acid-base reactions are usually written as:

$$>SuOH \Leftrightarrow > SuO^- + H^+ \tag{7}$$

Where $> SuOH, > SuO^-$ and $> Su$ represent the active groups as protonated and deprotonated and their substrate respectively. The acid/base constant associated to these sites is defined by:

$$K_a = \frac{[> SuO^-][H^+]}{[> SuOH]} \tag{8}$$

The total site (non-complexed site) concentration equals:

$$[> SuOH]_{tot} = [>SuOH] + [>SuO^-] \tag{9}$$

Consequently, the protonated site concentration is expressed by:

$$[>SuOH] = \frac{\frac{[> SuOH]_{tot} [H^+]}{K_a}}{\frac{1 + [H^+]}{K_a}} \tag{10}$$

Consequently, for a specific pH, and for a known Ka, it is possible to use Eq. 9 to calculate the concentration of sites suitable for complexation, from the total number of sites calculated using Eq. 6.

In the case where a second site is in the vicinity of a first one, it is possible that they participate in two acid-base reactions and may become coupled in the same fashion as in reaction {1}. This reaction becomes:

$$> (SuOH)_2 \Leftrightarrow > (SuO^-)_2 + 2 H^+ \tag{11}$$

This reaction would be quantified by a cumulative acid-base constant, $_{a(2)}$, defined by:

$$\beta_{a(2)} = \frac{[> (SuO^-)_2][H^+]^2}{[>(SuOH)_2]} \tag{12}$$

In a general case, of multi-site reactions, reaction {1} becomes:
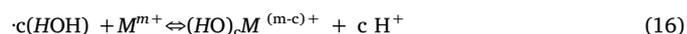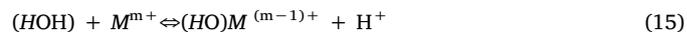
$$> (SuOH)_c \Leftrightarrow > (SuO^-)_c + c H^+ \tag{13}$$

The cumulative multi-acid-base constant is given by:

$$\beta_{a(c)} = \frac{[> (SuO^-)_c][H^+]^c}{[>(SuOH)_c]} \tag{14}$$

2.3. Hydroxo complexes properties

The acid base properties of metal ions are described by their build-up of hydroxo complexes on metal ions and their successive hydroxo complexes reactions:

$$(HOH) + M^{m+} \Leftrightarrow (HO)M^{(m-1)+} + H^+ \tag{15}$$

$$\cdot c(HOH) + M^{m+} \Leftrightarrow (HO)_c M^{(m-c)+} + c \, H^+ \tag{16}$$

When the equilibria are reached, the hydroxo complexation constants $K_{h(1)}$ and $\beta_{h(c)}$ associated to the reactions {4} and {5} are given as:

$$K_{h(1)} =$$

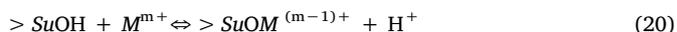$$K_{h(1)} = \frac{[(HO) M^{(m-1)}][H^+]}{[M^{m+}]} \tag{17}$$

and

$$\beta_{h(c)} = \frac{[(HO) c M^{(m-c)}][H^+]c}{[M^{m+}]} \tag{18}$$

with c = 2, 3, 4, 5 or 6. The cumulative hydrolysis constant, $\beta_{h(c)}$, as displayed in (18)

$$\beta_{h(c)} = \prod K_{h(1)}. \, K_{h(2)}). \, K_{h(3)}. \, .K_{h(c)} \tag{19}$$

2.4. Formation of surface complexes

On the surface structure, $> Su$, associated with one or several groups (c) also called dentate which are available to form with active groups $> (SuOH)_c$ a surface complex with a metal ion or a complex containing such an ion. The simplest case $(c = 1)$ is displayed in reaction {6}:

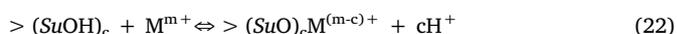$$> SuOH + M^{m+} \Leftrightarrow > SuOM^{(m-1)+} + H^+ \tag{20}$$

This reaction may be reversible under normal conditions as reported by Degueldre & McGowan [38] and the constant of surface complexation may be written as:

$$K_{s(0)} = \frac{[(>(SuO) M^{(m-1)+}][H^+]}{[> SuOH][M^{m+}]} \tag{21}$$
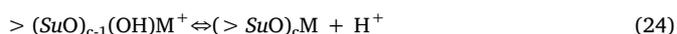
for the sorption of the naked ion.

In general case, bonds to several sites may occur, as per reaction {22}.

$$> (SuOH)_c + M^{m+} \Leftrightarrow > (SuO)_c M^{(m-c)+} + cH^+ \tag{22}$$

Where c denotes the dentate state. The cumulative constant of surface complexation may be written as:

$$\beta_{s(c)} = {}_c K_{s(c)} = \frac{[(>(SuO)_c M^{(m-c)+}][H^+]^c}{[(> SuOH)c][M^{m+}]} \tag{23}$$

It may also be that the metal or soluble complex may bind with additional sites after being bound to one or more initially as illustrated in {8}.

$$> (SuO)_{c-1}(OH)M^+ \Leftrightarrow (> SuO)_c M + H^+ \tag{24}$$

It is thus possible to adapt Eq. 17 to calculate a $K_{s(c)}$ for the concentration on the surface and in solution in mol g^{-1} and mol mL^{-1}, respectively. The equations (Eqs. 17 and 18) are related to the formation of mono- and multi-dentate complexes respectively. The multi-dentates are subdivided into bi- (2), tri-(3) and tetra- (4) dentates. However, it must be noted that not every complex can exist in every

state and in some cases the surface may not act as a tetra-dentate ligand for example.
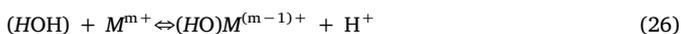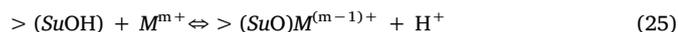
It should be noted that the organic molecules are a priori more flexible than the inorganic one, increasing the likelihood that multiple bonds (or "multidentate") could be made with a wider range of sizes of single ion or complexes than the rigid structures of the clay-like minerals.

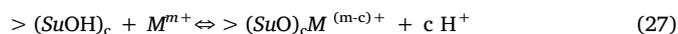## 2.5. Correlation for mono- and multi- dentate

In order for the metal or complex to form a surface complex, a consistent approach was suggested by Degueldre et al. [41] for prediction of stability constants of the surface complexes, $K_{s(0)}$, by correlating with the corresponding the hydrolysis constants $K_{h(1)}$ of the ions and complexes involved in the surface complexation states.

This analogy is ruled by the set of reactions {7} with {8}, and {9} with {10}.

The reaction couples that can be compared are:

$$> (SuOH) + M^{m+} \Leftrightarrow > (SuO)M^{(m-1)+} + H^+ \tag{25}$$

$$(HOH) + M^{m+} \Leftrightarrow (HO)M^{(m-1)+} + H^+ \tag{26}$$

for the mono-dentate, and

$$> (SuOH)_c + M^{m+} \Leftrightarrow > (SuO)_c M^{(m-c)+} + c\,H^+ \tag{27}$$

$$\cdot c(HOH) + M^{m+} \Leftrightarrow (HO)_c M^{(m-c)+} + c\,H^+ \tag{28}$$

for the multi-dentate.

The analogy between reactions {9} and {4} was proposed and the following relation suggested:

$$LogK_{s(0)} = T_m + S_m LogK_{h(1)} \tag{29}$$

where S_m and T_m are surface-specific constants.

In previous work, this relation was limited to mono-dentate such as in Degueldre et al. [40]. Analysis of multi-dentate constants has shown however that successive multi-dentate can be described by the same relation form as Eq. (19), with the successive hydrolysis constants of the element, but that these constants are specific to the dentate state: so an active site will have mono-, bi-, tri- and tetra- values of $S_{m(c)}$ and a mono-, bi-, tri- and tetra- values of $T_{m(c)}$, where the correlations are due to the analogy between reactions {10} and {5}. The correlation coefficients $S_{m(c)}$ and $T_{m(c)}$ are then unique surface-specific constants, in each state.

$$Log\,K_{s(c-1)} = T'_{m(c)} + S'_{m(c)} Log\,K_{h(c)} \tag{30}$$

Where c is the dentate state for the individual surface complexation constant $K_{s(c+1)}$ and for the hydration constant for $K_{h(c)}$. In these correlation plots, $S_{m(c)}$ represents the impact of an increasing complexation binding strength with the hydroxide complexation and the values of $T_{m(c)}$ follows the initial threshold required to make initially the bond.
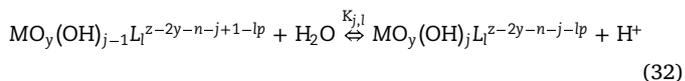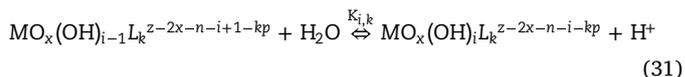
The relation was earlier limited to mono-dentate as investigated by Degueldre et al. [40,41]. However several authors have shown that multi-dentates are common e.g. Carbonaro et al. [42], Loiseau et al. [43]. In case of organic molecules $> SuOH$ active groups are more flexible than the inorganic one, e.g. $> SiOH$, $> FeOH$ and $> AlOH$ leading to a binding with a larger degree of freedom for the considered ions or complexes. They are known to flex around complexes, leading to stronger S_m values. However, counter effects would also expect difficulties, such as the lack of suitable sites, which would be reflected in lower T_m values.

It should be noted that the logarithmic plots displays of the successive logarithm of the mono- hydroxide complexation constants with the logarithm of the mono-dentate surface complexation constants, as well as the logarithm of a given multi- hydroxide complexation constants with the corresponding multi-dentate surface complexation constants, allowed observation of linear relationships between these stability constants, which are surface site specific.
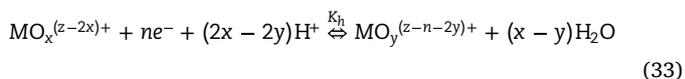
2.6. Complexes formation in the redox range

The hydrolysis stability constants of both redox species ($K_{h(i,k)}$ for oxidising and $K_{h(j,l)}$ for reducing species) can be evaluated for the stepwise reactions {4} and {6}. It should be noted that the notation is intended to include both oxocation and non-oxocation species.

Further complications due to metal complexation by k-ligands (L^{-p}) or L-ligands (L^{-p}) such as carbonates, were also considered. The complexation reactions in solution for both redox species read as:

$$MO_x(OH)_{i-1}L_k^{z-2x-n-i+1-kp} + H_2O \overset{K_{i,k}}{\Leftrightarrow} MO_x(OH)_iL_k^{z-2x-n-i-kp} + H^+ \tag{31}$$

$$MO_y(OH)_{j-1}L_l^{z-2y-n-j+1-lp} + H_2O \overset{K_{j,l}}{\Leftrightarrow} MO_y(OH)_jL_l^{z-2y-n-j-lp} + H^+ \tag{32}$$

Therefore, it is possible to describe the generalised redox couple $MO_x^{(z-2x)+}/MO_y^{(z-n-2y)+}$ (where $MO_x^{(z-2x)+}$ is the oxidised species and $MO_y^{(z-n-2y)+}$ the reduced one), by reaction {13}.

$$MO_x^{(z-2x)+} + ne^- + (2x-2y)H^+ \overset{K_h}{\Leftrightarrow} MO_y^{(z-n-2y)+} + (x-y)H_2O \tag{33}$$

The surface complexation for the hydrolysed (and complexed) species is described by reactions {6} and/or {7}, considering the generalised quasi-neutral site $> SuOH$. The surface complexation constants are $Ks(i,k)$ for the oxidising species and $Ks(j,l)$ for the reducing species. The indices k and l refer to the relevant co-ordination numbers of the metal ions, in the context of those selected ligands. Furthermore, effects of the redox potentials in solution and at the surface are taken into account by reactions {15} and {16}.

▲

.

When the reactions are written in terms of free metal M^{z+}, the cumulative constants are β_i and β_j, respectively ($\beta_{i\,or\,j} = \beta_{1.i\,or\,j} = \Pi K_i$ where I or j = 0, 1,.).

The ratio between the concentrations of both redox species is written as a function of the redox potential (E) by applying the Nernst Eq. (21):

$$E = E° + (2x - 2y + i - j)RT(nF)^{-1}\ln[H^+] + RT(nF)^{-1}\ln$$

$$\left\{ [MO_x^{(z-2x)+}][MO_y^{(z-n-2y)+}]^{-1} \right\} \tag{34}$$

Where the apparent standard redox potential ($E'°$) is linked to the standard redox potential ($E°$) in water according:

$$E'° = E° + (2x - 2y + i - j)RT(nF)^{-1}\ln[H^+] \tag{35}$$

Rearranging these equations by considering surface complexation for both redox forms and including concurrent complexation with ligands as formulated in the above-mentioned equations and reactions lead K_d (from Eq.2) to be written in terms of the redox potential, and evaluated by Eq. (24).

$$K_d = \frac{\left\{ \sum_{i,k}\left[\frac{K_{s,i,k}\cdot\beta_{i,k}\cdot[L_k]^k}{[H^+]^i}\right] + \sum_{j,l}\left[\frac{K_{s,j,l}\cdot\beta_{j,l}\cdot[L_l]^l}{[H^+]^j}\right] \exp(A)\right\}\cdot\frac{[>SuOH]}{[H^+]}}{\left\{ \sum_{i,k}\left[\frac{\beta_{i,k}\cdot[L_K]^k}{[H^+]^i}\right] + \sum_{j,l}\left[\frac{\beta_{j,l}\cdot[L_l]^l}{[H^+]^j}\right]\cdot\exp(A)\right\}\cdot[part]} \tag{36}$$

where $A = \dfrac{(E'° - E)nF}{RT}$ and the sorbing particle concentration [part] is given in g.L^{-1}. The free ligand concentration [L] can be written in terms of the total ligand concentration (mol L^{-1}).

The formulation of Eq. (23) implies occurrence of linear adsorption isotherms (of Langmuir type, see Eq. 2) and no saturation effects. It

Table 1

Hydrolysis constants and standard redox potentials of uranium (NEA [44] and Grenthe et al. [45]).

4i or j	pKh U (III)	E° (V)	pKh U (IV)	E° (V)	pKh U (V)	E° (V)	pKh U (VI)	E° (V)
= 1	6.80	0	0.54	-0.553	0.00	0.053	0.00	0.006
= 2	7.30	0	0.70	-0.553	11.30	0.053	5.25	0.006
= 3	11.60	0	3.60	-0.553	12.30	0.053	6.90	0.006
= 4	14.35	0	5.30	-0.553			8.10	0.006
= 5			13.10	-0.553			12.15	0.006

should be noted that no electrostatic effects and no activity corrections were considered at this stage.

Any K_d calculated on this basis Eq. (23) can be evaluated for a given pH at any specific value of E.

Eq. (23) can further be extended by considering sorption on different multi-dentate groups, utilising the appropriate cumulative constant. For the bidentate surface complexes the $K_{d(bi)}$ becomes:

$$K_{d(bi)} = \frac{\left\{ \sum_{m,n}\left[\frac{K_{s,m,n}\cdot\vartheta_{m,n}[L_n]^n}{[H^+]^m}\right] + \sum_{o,p}\left[\frac{K_{s,o,p}\cdot\vartheta_{o,p}\left[L_p\right]^p}{[H^+]^o}\right]\exp(A) \right\}\frac{[>(SuOH)c]}{[H^+]c}}{\left\{ \sum_{m,n}\left[\frac{\vartheta_{m,m}[L_n]^n}{[H^+]^m}\right] + \sum_{o,p}\left[\frac{\vartheta_{o,p}\left[L_p\right]^p}{[H^+]^o}\right]\exp(A) \right\}[part]}$$

(37)

For the multi-dentate complexes the formulation is similar to that described for mono-dentate, however c protons are exchanged instead of 1. Since the same metal species are considered, m, o, n and p will match those of i, j, k and l, respectively. As stated earlier, these values are cumulative and represent a mixed species collective.

As independent processes, a total net K_d ($K_{d(net)}$) which represents every species in solution, and every form of multi-dentate surface complexes, is calculated by Eq. (25).

$$K_{d(net)} = K_{d.\,mono-} + K_{d.\,bi-} + K_{d.\,tri-}$$

(38)

The following assumptions were made for the application of the proposed model:

- The surface complexation reactions occur under equilibrium.
- There are no kinetics effects considered.
- The sorption isotherms are of Langmuir type.
- The model applies pure surface complexation with no interference of the charges of the particles.

- There is no reaction coupling that could lead to irreversible sorption e.g. surface complexation & aggregation.

The model would be arranged accordingly in case of the sorption is also driven by these conditions.

3. Data needed for model application

The model generic application requires data from the liquid phase and from the solid sorbent. It is then applied for the sorption of uranium from seawater on biomass material supposed to be covered by carboxylic active groups.

3.1. Liquid environment

The data required for uranium speciation in water are the pKh for each of its hydroxo complexes and the E° for each of its redox couples. These data are as listed in the Table 1.

In carbonated water the build-up of carbonate complexes must be taken into account. The pK$_h$ for each of the hydrolysis constants and E (V) are listed by order of number of carbonating- ligands in Table 2.

3.2. Solid covered with carboxylic groups

A review of stability constant data of transition metals, lanthanides and actinides (d and f elements) complexes with carboxylic ligands has first been carried out. The carboxylic groups ranged from methanoic (formic), to butanoic, and hexanoic, and the correlations between stability constant and respective hydroxide complexes are shown Fig. 1.

Data were collected from the literature, however it was noted that the source of data was not sufficiently large and that it often originated from various methodologies, leading occasionally to inconsistent results. The data were considered without validation, leading to minor variation in herein testing conditions (Martell & Smith [46]). Most values reported for stability constants and hydrolysis constants were

Table 2

Hydroxo complex constants and standard redox potentials of uranium carbonated states (NEA [44] and Grenthe et al. [45]).

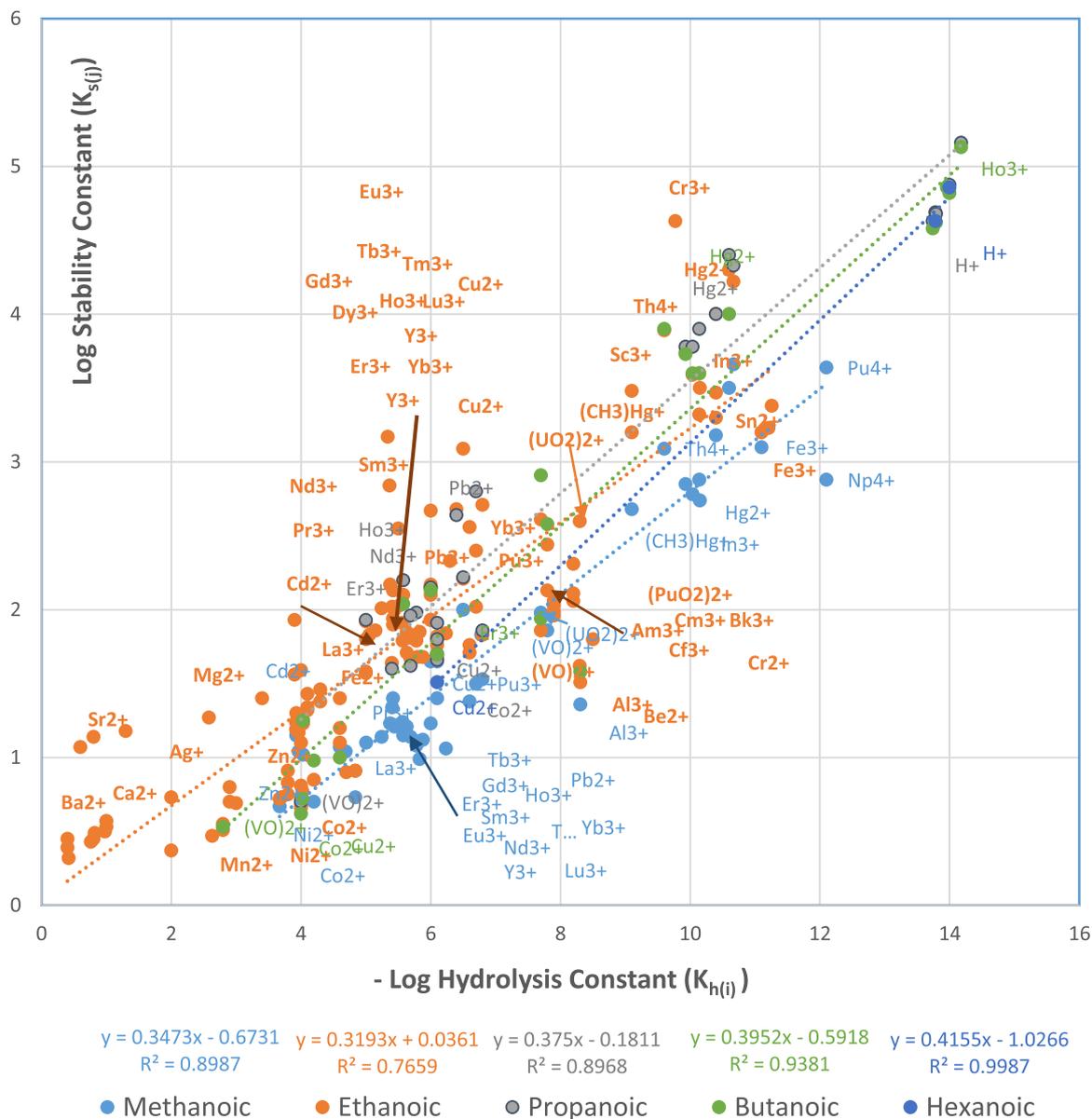| i & l (for K $_{(i,l)}$)	pK$_h$ U (III)	E° (V)	j & l (for K $_{(j,l)}$)	pK$_h$ U (IV)	E° (V)
i = 0, l= 1/ 2/ 3	5.12 /1.80 / − 1.90	0	j = 0, l= 1/ 2/ 3/ 4	6.5/ 5.3/ 1.6/ − 3.4	-0.553
i = 1, l= 0	-11.3	0	j = 1, l= 0/1/2	-6.8 /− 5.8 /− 7.8	-0.553
i = 2, l= 0	-12.3	0	j = 2, l= 0/1	-7.3/ − 7.9	-0.553
			j = 3, l= 0	-11.6	-0.553
			j = 4, l= 0	-14.35	-0.553
j & l (for K$_{j,\,l}$)	**pK$_h$ U(V)**	**E° (V)**	**j & l (for K$_{j,\,l}$)**	**pK$_h$ U(VI)**	**E° (V)**
j = 0, l= 1/ 2/ 3/ 4	13.7/ 10.6/ 7.6/ 3.3	0.053	j = 0, l= 1/ 2/ 3/ 4	9.94/6.67/ 5.23/7.6/ 3.3	0.006
j = 1, l= 0	-0.54	0.053	j = 1, l= 0	-5.25	0.006
j = 2, l= 0	-0.7	0.053	j = 2, l= 0	-6.9	0.006
j = 3, l= 0	-3.6	0.053	j = 3, l= 0	-8.1	0.006
j = 4, l= 0	-5.3	0.053	j = 4, l= 0	-12.15	0.006
j = 5, l= 0	-13.1	0.053			

Fig. 1. Comparison of correlation between carboxylic mono-dentate surface complexation constants of various metals and their respective hydroxide complexation constants.

tested at 25 °C, but some variations due to operating temperature between 18 °C and 32 °C were included. More ranging variability stem from the range of ionic strength of solution which would lead them to deviate from the reference used for the hydrolysis constant. In cases where corresponding conditions were not available, values were computed by simple mathematical interpolation by using those that were available.

Furthermore, data on multi-dentate interactions were not fully distributed across the dataset, leading to more challenging extrapolation. These interactions have however limited the calculation of $T_{m(c)}$ and $S_{m(c)}$ to the mono and bidentate forms. The tri-dentate values were calculated and displayed with similar characteristics, but the confidence intervals were found relatively large. The tetra-dentate relation was considered, but was later discarded due to the very low availability of source of data and these observations applied to the tri-dentate values as well.

The correlations between the Log stability constant for poly-dentate complexes of various metals on ethanoic acid surface groups, with the

Log of the corresponding hydrolysis constant are shown in Fig. 2 for mono-dentate complexes of various metals, for bi-dentate complexes and for tri-dentate complexes. Here again data were gained from Martell & Smith [46].

Conditions: data from Martell & Smith [46].

Conditions: data from Martell & Smith [46].

For the purposes of mapping the relationship, the Log of the hydrolysis constant was compared to the Log of the stability constant. It showed that the predicted relationship was linear (with the majority of trend line fits exhibiting an R^2 greater than 0.8 for first and second ligands on the five acids, with one exception), with the trend lines forming a regular series. Methanoic acid proved to be exceptional with regard to this relationship, but for longer chains, a S_m of between 0.3 and 0.4 was shown to be consistent across the series.

The reduced gradient exhibited by methanoic acid is most likely an exception, stemming from a result of water/acid component interactions with the reagents in solution, creating more complicated environment at the microscale. As these effects are less relevant for the

Fig. 2. Correlation between the Log stability constant for poly-dentate complexes of various metals on ethanoic acid surface groups, with the Log of the corresponding hydrolysis constant. **a.** for mono-dentate complexes of various metals, to the Log of their first hydrolysis constant. **b.** for bi-dentate complexes of various metals, to the Log of their second hydrolysis constant, **c.** for tri-dentate complexes of various metals, to the Log of their third hydrolysis constant.

Table 3
T_m of various carboxylic acids, for the 1st to 4th dentate binding complex. Conditions: data extracted from Fig. 1 and Fig. 2a,b,c.

T_m	Methanoic	Ethanoic	Propanoic	Butanoic	Hexanoic
1st	0.0453	0.0077	-0.527	-0.2516	-1.0266
2nd	-1.1295	-1.2508	-3.037	-1.3621	
3rd	-2.376	-5.0538			
4th	0.0191	-4.0819			

Table 4
S_m of various carboxylic acids, for the 1st to 4th dentate binding complex. Conditions: data extracted. from Fig. 1 and Fig. 2a,b,c.

S_m	Methanoic	Ethanoic	Propanoic	Butanoic	Hexanoic
1st	0.2574	0.331	0.3981	0.3633	0.4155
2nd	0.298	0.3932	0.4668	0.3439	
3rd	0.3336	0.5967			
4th	0.1938	0.5599			

longer chains, they were discounted from the model, as they would represent non negligible deviations for the purposes of calculating the stability of methanoates.

The minimum energy threshold T_m displayed a linear relationship with the chain for the first and second binding of ligands, with the exception to the second ligand of propanoate. The fit of this trend line was poor (R^2 of 0.72). These are displayed in Table 3. The slope S_m of these linear plots are given in Table 4.

This pattern appears to be caused by the bond strength which is consistent with the forms and dictated by the carboxylic "head", while the length of chain would affect the initial energy requirement: this is possibly due to restrictions on the angle of incidence that makes the initial contact, or the probability of correct orientation in the plane. This would also illustrate the relation as the binding increases, since the third and fourth bonds necessarily need to form from a different surface complex, which would significantly reduce the likelihood to have a simple mechanism for decoupling from the surface.

While the correlation coefficients for tri- and tetra- dentate were not available for propanoic and butanoic acid derived ligand, specific values were available for some metals at higher chain lengths. The calculated values for U_2O^{2+} is found below the known actual values, but is within the R^2 values.

Based on this, it was decided that ethanoic acid would be sufficiently representative for the structural repeating unit for longer, more complex mono acids, or poly acids with short inter site chain lengths. While the predicted value for these larger structures have limited data availability, it is a reasonable that from the available data it could be possible to modify the relation.

The minimum energy threshold Tm(c) and the slope Sm(c) values for ethanoic acid used for the simulations are given in Table 5. The standard deviation on the minimum energy threshold is given by = (1/ N) [Σ(y-ŷ)²]^{1/2} with N number of data, y: data value and ŷ data obtained by regression.

Table 5
Tm(c) and Sm(c) values for ethanoic acid used for the simulation Conditions: data from Martell & Smith nc not calculated.

Dentate (c)	$T_{m\ (c)}$ ±	$S_{m\ (c)}$	N
Mono	0.0077 ± 0.0541	0.331	110
Bi	-1.25 ± 1.81	0.3932	32
Tri	-5.05 ± 1.68	0.5967	13
Tetra	-4.08 ± nc	0.5599	.nc

3.3. Specific application

In order to make the work relevant to an ongoing experimental work, the sorbent materials was assumed to consist of spherical particles 0.2 mm in diameter, with a total concentration of $30\ g\,L^{-1}$. The interactive plane of ethanoic acid was assumed to be the dimensions of the molecular form, which is $0.4 \times 1.3\ nm$ in size, with 1 site, as the monomer is the most common form of unit of ethanoic acid crystallisation as reported by Jones & Templeton [47]. The particle bulk was assumed to have the standard density: $1.05\ g\,cm^{-3}$, an active group molecular mass of $60.052\ g\,mol^{-1}$, and a pK_a of 4.756. This gives a site density of 2 sites per nm^2, equating to an average site concentration of $4.36 \times 10^{-8}\ mol\,g^{-1}$, the later being corrected in Eq. 5 for the inactive fraction of the surface I which is fixed 0.5 here. All the values are based on standard conditions, i.e. temperature: 25 °C and pressure: 1 Atm where appropriate. The K_s correlation values calculated previously for the ethanoic acid unit are given by Eq. (20) using data given in Table 5.

The model is subsequently applied to the sorption of uranium from seawater. In this case the concentration of uranium has been found to be $3 \times 10^{-9}\ g\,L^{-1}$ (3 ppb) that is the 'nominal' value in marine environment, e.g. Millero [48]. The pH of seawater used for calculations is about 8.0. For example Rérolle et al. [49]&[50] reported pH values between 7.995 and 8.210 for Irish Sea water (for T: 8–26 °C) and a redox potential of about + 0.4 V in surface conditions.

For the seawater environment, the total carbonate concentration has been assumed to be $2.2 \times 10^{-3}\ mol\,L^{-1}$ and their first and second Log coefficients to be 10.329 and 16.681 (e.g. Table 2), respectively (Sharp et al. (2017) [51]).

4. Results

The uranium Kd vs E diagrams for fixed pH were replotted as proposed in Degueldre & McGowan [38] in the case of carbonate free solution followed by carbonated solutions. In all cases and to mimic the tests performed in McGowan et al. [16], the particle concentration is $30\ g\,L^{-1}$ and the site density is $2.18 \times 10^{-8}\ mol\,g^{-1}$ after correction in Eq. 5 for the inactive fraction of the surface, which is fixed at 0.5.

4.1. Kd calculations, effect of pH and E for mono-, bi- and tri- carboxylic group complexes

The K_d (mL g^{-1}) for uranium surface complexation by **individual carboxylic groups** on bioorganic particles in a carbonate free environment as a function of redox potential for various pH values was
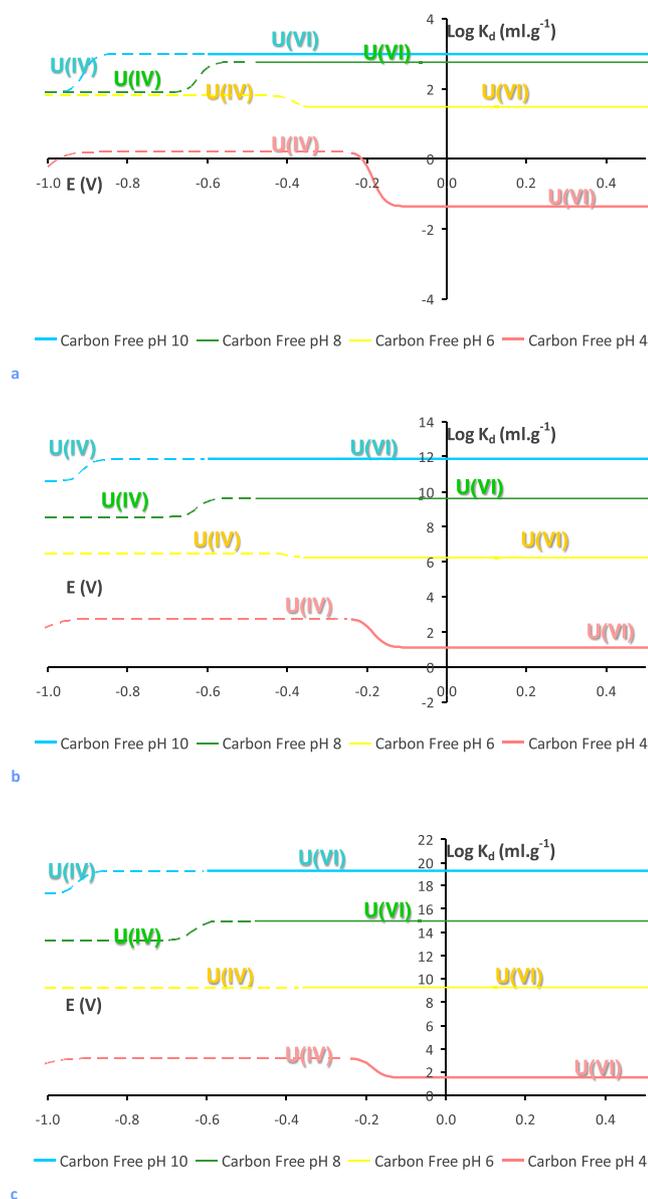
Fig. 3. Uranium sorption coefficient Kd (mL g-1) as a function of potential for various pHs. **a.** on mono-dentate carboxylic (ethanoic) group loaded particles. **b.** on bi-dentate carboxylic (ethanoic) group loaded particles. **c.** on tri-dentate carboxylic (ethanoic) group loaded particles. *Conditions: particles of 0.2 mm diameter, potential vs NHE, site density: 2 nm^{-2}, carbonate free. Solid lines: in the water redox stability domaine, dashed line: outside the water redox stability domaine.*

first calculated. The surfaces of the particles of 0.2 mm diameter are covered by ethanoic groups forming first mono-dentate complexes with U(VI) and at lower E values U(IV). In this case, the calculations were done using the correlations with T_m and S_m given listed in Table 5 for mono-dentates. The results are plotted in Fig. 3.a.

At pH 4 and in oxidative conditions, the Log K_d values are found at −1.3 for U(VI) (here from −0.1 to +0.96 V) and at the apparent redox potential (−0.26 V) Log K_d has increased to +0.2 for U(IV).

Subsequently, at pH 6 and in oxidative conditions, Log K_d values are found at +1.5 for U(VI) (from −0.36 to +0.84 V) and at the apparent redox potential of −0.48 V Log K_d increases up to +1.8 for U(IV). The later reduction takes however place below the redox stability domain of water.

Later, at pH 8 and in oxidative conditions, Log K_d is found at +2.8 for U(VI) (from −0.48 to 0.72 V), below the minimum apparent redox

potential (−0.48 V) it decreases down to +1.9 for U(IV) (from −0.48 to −0.62 V). This reduction start however outside the redox stability domain of water.

Finally, at pH 10 and in oxidative conditions, Log K_d is found at +3.0 for U(VI) (−0.60 to +0.60 V) and below the minimum apparent redox potential (−0.60 V) Log K_d decreases down at +1.9 for U(IV) for −0.96 V.

The K_d (mL g^{-1}) for uranium surface complexation by **two carboxylic groups** on bioorganic particles was then calculated again in carbonate free environment as a function of redox potential for various pH's. The surfaces of the particles of 0.2 mm diameter were covered by ethanoic groups forming bi-dentate complexes with U(VI) and at lower E values with U(IV). Calculations were done using the correlations with T_m and S_m given in Table 5 for bi-dentates. The results are plotted in Fig. 3.b.

At pH 4 and in oxidative conditions (−0.15 to +0.96 V), Log K_d values are found at +1.1 for U(VI). Below the apparent redox potential Log K_d increases up to +2.7 for U(IV) (from −0.15 to −0.23 V) just prior the water stability limit (−0.24 V).

Further, at pH 6 and in oxidative conditions, Log K_d values are found at +6.2 for U(VI) in the redox range −0.3 to +0.84 V Log K_d decreases down to +6.5 for U(IV) (at −0.43 V, i.e. below the stability limit of water (−0.36 V).

Follow then at pH 8, in oxidative conditions, Log K_d becomes +9.6 for U(VI) in the domain −0.57 to +0.72 V and then it decreases down to +8.6 for U(IV) at −0.66 V (i.e. below the water stability limit of −0.48 V) and below.

And finally, at pH 10 and in oxidative conditions, Log K_d is found at +11.9 for U(VI) and below the apparent redox potential (−0.84 to +0.60 V) Log K_d decrease down to +10.6 for U(IV) at −0.95 V (below −0.60 V the water limit) and below.

The K_d (mL g^{-1}) for uranium surface complexation by **three carboxylic groups** on bioorganic particles was then calculated in carbonate free environment as a function of redox potential for various pH's. The surfaces of the particles of 0.2 mm diameter are covered by ethanoic groups, forming tri-dentate complexes with U(VI) and at lower E values with U(IV). Calculations were done using the correlations with Tm and Sm given in Table 5 for tri-dentates. The results are plotted in Fig. 3.c.

At pH 4 and in oxidative conditions, Log K_d is found at +1.5 for U(VI) and for the apparent redox potential range: −0.16 to +0.96 V. It then increases up to +3.2 for U(IV) at −0.24 V, i.e. at the reduction limit of water.

Then at pH 6, in oxidative conditions, Log K_d is found at +9.3 for U(VI) in the potential range going from −0.35 to +0.84 V, and would decrease slightly down to +9.2 for U(IV) at −0.43 V, below the water redox limit −0.36 V.

At pH 8 and in oxidative conditions, Log K_d is found at +15.0 for U(VI) in the redox domain (−0.54 to +0.72 V) and then decreases to +13.3 for U(IV) at −0.68 V again below the water limit (−0.48 V).

At pH 10 and in oxidative conditions, Log K_d is found at +19.3 for U(VI) from the apparent redox potential +0.6 down to −0.85 V and should increases subsequently up to +17.4 for U(IV) at −0.95 V.

4.2. Kd calculations, effect of pH and E for mono-, bi- and tri- carboxylic group complexes, effect of carbonate

The K_d (mL g^{-1}) for uranium surface complexation by **single carboxylic groups** on bioorganic particles was first calculated in a 2×10^{-3} M carbonate suspension (i.e. seawater case at pH 8) as a function of redox potential for various pH's. The surfaces of the particles of 0.2 mm diameter are covered by ethanoic groups, forming mono-dentate complexes with U(VI) and at lower E values U(IV). Calculations were first done using the correlations with Tm and Sm given in Table 5 for mono-dentates. The results are plots are plotted in Fig. 4.a.
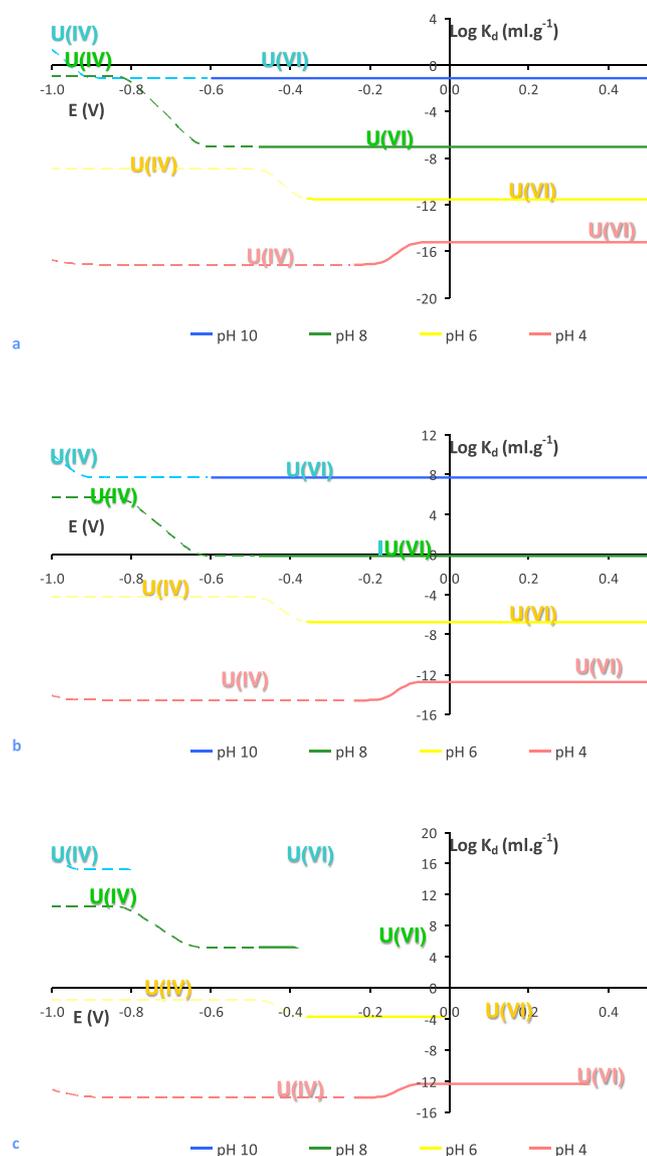
Fig. 4. Uranium sorption coefficient K_d (mL g^{-1}) as a function of potential for various pHs. **a.** on mono-dentate carboxylic (ethanoic) group loaded particles. **b.** on bi-dentate carboxylic (ethanoic) group loaded particles. **c.** on tri-dentate carboxylic (ethanoic) group loaded particles. Conditions: particles of 0.2 mm diameter, potential vs NHE, site density: 2 nm^{-2}, 2.2×10^{-3} M total carbonate concentration. Solid lines: in the water redox stability domain, dashed line: outside the water redox stability domain.

At pH 4 and in carbonated conditions, Log K_d is found at − 15.2 for U (VI) (from −0.06 to 0.96 V) and below the apparent redox potential of − 0.06 V it transitions down to − 17.1 for U(IV) (at −0.25 V).

For pH 6, in carbonated conditions, Log K_d is observed at − 11.5 for U(VI) (from −0.34 to +0.84 V.). It then increases up to − 8.9 for U (IV). Below − 0.48 V however, these values are below the reduction limit of water (−0.36 V).

Further at pH 8 and in carbonated conditions, Log K_d is found at − 7.0 for U(VI) for the apparent redox potential ranging from − 0.48 to + 0.72 V. It would then transit up to − 093 for U(IV), however this would be below the redox stability limit of water (−0.48 V).

Finally, at pH 10, in carbonated conditions, Log K_d is found at − 1.1 for U(VI) (from −0.6 to 0.60 V) in the apparent redox potential range (−0.60 to +0.60 V), it would increase up to − 0.8 for U(IV) below − 0.7 V.

The K_d (mL g^{-1}) for uranium surface complexation by **double carboxylic groups** on bioorganic particles was first calculated in a

2×10^{-3} M carbonate suspension as a function of redox potential for various pH's. The surfaces of the particles of 0.2 mm diameter are covered by ethanoic groups, forming bi-dentate complexes with U(VI) and at lower E values U(IV). Calculations were first done using the correlations with T_m and S_m given in Table 5 for bi-dentates. The results are plots are plotted in Fig. 4.b.

At pH 4, in carbonated conditions, Log K_d is found at − 12.7 for U (VI) for the apparent redox potential going from − 0.10 to + 0.96 V. It then transitions down to − 14.6 for U(IV) at − 024 V (water stability limit).

Subsequently, at pH 6, in carbonated conditions, Log K_d is found at − 6.8 for U (VI) for the apparent redox potential range − 0.36 to + 0.84 V. It then increases up to − 4.3 for U(IV) at − 0.50 V.

For pH 8, in carbonated conditions, Log K_d becomes − 0.15 for U (VI), for the apparent redox potential going from − 0.59 to + 0.72 V. It then increases up to + 5.8 for U(IV) (−0.84 V i.e. below the water stability limit).

Finally, at pH 10, in carbonated conditions, Log K_d reaches the value of + 7.8 for U(VI) for the apparent redox potential, going from − 0.60 to + 0.60 V and before the formation of U(IV) (below −0.90 V).

The K_d (mL g^{-1}) for uranium surface complexation by **triple carboxylic groups** on bioorganic particles was first calculated in a 2×10^{-3} M carbonate suspension as a function of redox potential for various pH's. The surfaces of the particles of 0.2 mm diameter are covered by ethanoic groups forming tri-dentate complexes with U(VI) and at lower E values U(IV). Calculations were first done using the correlations with T_m and S_m given in Table 5 for tri-dentate. The results are plots are plotted in Fig. 4.**c.**

At pH 4, in carbonated conditions, Log K_d is found at − 12.3 for U (VI) for the apparent redox potential of − 0.06 to + 0.96 V. It then transitions down to − 14.1 for U(IV) at − 0.21 V just above the water limit (−0.24 V).

Then, at pH 6, in carbonated conditions, Log K_d is found to be − 3.7 for U (VI) in the apparent redox potential ranging from − 0.33 to + 0.84 V. It then increases up to − 1.5 for U(IV) at − 0.48 V, below the water limit (−0.36 V).

For pH 8, in carbonated conditions, Log K_d is to be found at + 5.2 for U(VI) above the apparent redox potential of − 0.6 to + 0.72 V. It would then increase up to + 10.5 for U(IV) at − 0.86 V. This would be below the water limit of − 0.48 V.

Finally, at pH 10, in carbonated conditions, Log K_d becomes + 15.2 for U (VI) for the apparent redox potential range: − 0.88 to + 0.60 V. It would increase up to + 16.7 for U (IV) at − 1.06 V. This reduction would however take place below the stability of water (−0.60 V) at this pH.

4.3. Kd calculations under varying carbonate concentrations

The K_d (mL g^{-1}) for uranium surface complexation by a **single carboxylic group** on bioorganic particles was calculated in a carbonate suspensions which vary between 0, 2.2×10^{-6} and 2.2×10^{-0} or 2.2 M as a function of redox potential for pH 8.0. This range was selected as it provides reasonable values of surface carbonate concentrations and pH in the Irish Sea (e.g. Rérolle, et al. [48]). The surfaces of the particles of 0.2 mm diameter are covered by ethanoic groups, forming mono-dentate complexes with U(VI) and at lower E values with U(IV). Calculations were first done using the correlations with T_m and S_m given in Table 5 for mono-dentates. The results are plotted in Fig. 5a.

For carbonate concentrations below 2.2×10^{-6} M, the Log K_d is consistent, at ~2.8. As the carbonate concentration rises, it increasingly interferes with the surface complex formation, reducing the K_d. This K_d change is observed for U(IV) and U(VI).

It then begins a transition to the U(VI) associated K_d, which is much more displaced by the presence of the carbonates. Each order of
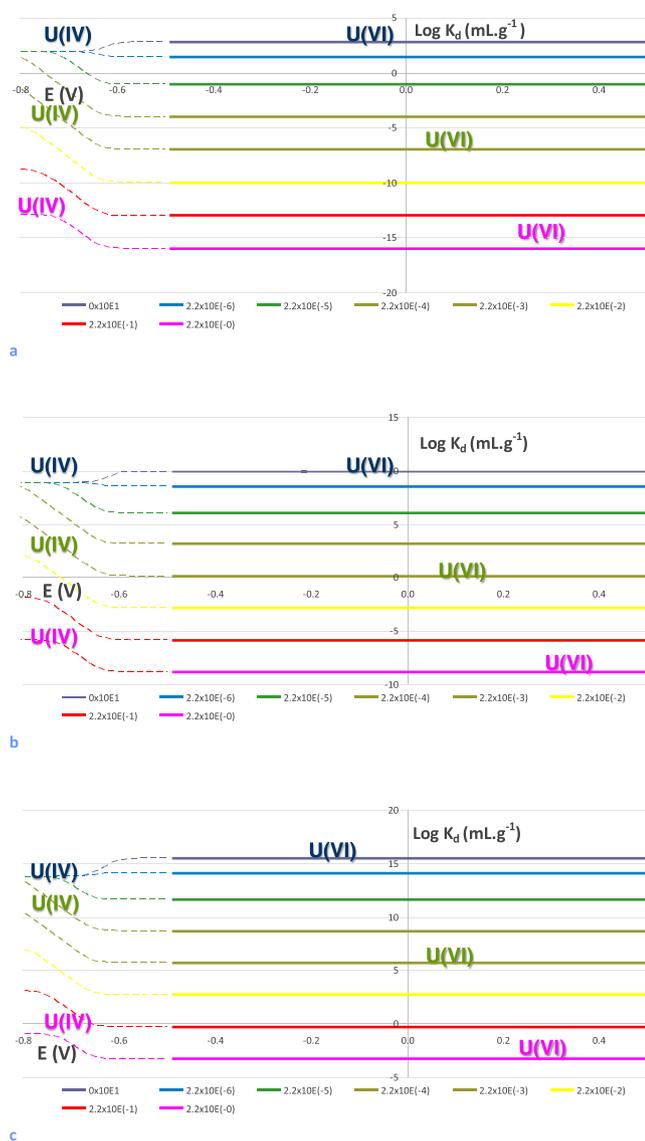
Fig. 5. Uranium sorption coefficient K_d (mL g^{-1}) as a function of potential for pH 8.0 and over varying carbonate concentrations. **a.** on mono-dentate carboxylic (ethanoic) group loaded particles. **b.** on bi-dentate carboxylic (ethanoic) group loaded particles. **c.** on tri-dentate carboxylic (ethanoic) group loaded particles.

magnitude increase in carbonate concentration decreases the log K_d by about 3.

The U(IV)/U(VI) point of transition, E'°, is consistent at around -0.60 V, but the inflexion point varies: the most negative point

Table 6

Transition point E'° and log K_d's (mL g^{-1}) for U(VI) and U(IV) sorption on mono-dentate carboxylic groups varying the total carbonate concentration at pH 8.

CO$_3$ Conc. (M)	U (VI) Log K$_d$	U (IV) Log K$_d$	U (IV)/U (VI) E$'^\circ$ (V)
0.0010ˆ+0X	+ 2.8	+ 1.9	-0.60
2.20E-06	+ 1.4	+ 1.9	-0.60
2.20E-05	-1.1	+ 1.9	-0.66
2.20E-04	-4.0	+ 1.2	-0.71
2.20E-03	-7.0	-2.0	-0.71
2.20E-02	-10	-5.0	-0.70
2.20E-01	-13	-8.9	-0.69
2.20E+00	-16	-12	-0.68

Table 7

Transition point E'° and Log K_d's (mL g^{-1}) for U(VI) and U(IV) sorption on bi-dentate carboxylic groups varying the carbonate concentration at pH 8.

Carbonate Conc. (M)	U (VI) Log K$_d$	U (IV) Log K$_d$	U (IV)/U (VI) E$'^\circ$ (V)
0.0010ˆ+0X	+ 9.9	+ 8.8	-0.63
2.20E-06	+ 8.5	+ 8.8	-0.63
2.20E-05	+ 6.0	+ 8.8	-0.67
2.20E-04	+ 3.1	+ 8.2	-0.71
2.20E-03	+ 0.1	+ 5.5	-0.73
2.20E-02	-2.9	+ 1.9	-0.71
2.20E-01	-5.9	-2.0	-0.70
2.20E+00	-8.9	-5.9	-0.68

$(-0.72$ V) being found for a carbonate concentration of 2.2×10^{-3} M. This is due to the presence of the U(VI) carbonato complexes. At higher carbonate concentrations, U(IV) starts to form complexes increasing the apparent standard redox potential of the couple. It must be noted that all the redox domains, where U(IV) forms, are below the stability limits of water i.e. -0.48 V. (Table 6).

The K_d mL g^{-1}) for uranium surface complexation by **two carboxylic groups** on bioorganic particles was calculated in a carbonate suspensions which varies between 0, 2.2×10^{-6} and 2.2×10^{-0} (or 2.2) M as a function of redox potential for pH 8.0. Calculations were first done using the correlations with T_m and S_m given in Table 5 for bidentates. The results are plotted in Fig. 5b.

For carbonate concentrations below 2.2×10^{-6}, the Log K_d is consistent, at ~ 9.9. As the carbonate concentration rises, it increasingly interferes with the binding, reducing the K_d. This K_d would be associated with U(IV).

It then begins a transition to the U (VI) associated K_d, which is much more displaced by the presence of the carbonates. For each order of magnitude increase in concentration the log K_d decreases by about 3.

U(IV)/U(VI) point of transition, E'°, is consistent at around -0.63 V, but the inflection point varies: the most negative point $(-0.73$ V) being found for a carbonate concentration of 2.2×10^{-3} M. This is due to the presence of the U(VI) carbonato complexes. At higher carbonate concentrations, U(IV) starts to form complexes increasing the apparent standard redox potential of the couple. Here again all the redox domains, where U(IV) forms are below the water stability limits i.e. -0.48 V. (Table 7).

The K_d (mL g^{-1}) for uranium surface complexation by **three carboxylic groups** on bioorganic particles was calculated in a carbonate suspensions which varies between 0, 2.2×10^{-6} and 2.2×10^{-0} M as a function of redox potential for pH 8.0. The surfaces of the particles of 0.2 mm diameter are covered by ethanoic groups, forming tri-dentate complexes with U(VI) and at lower E values U(IV). Calculations were first done using the correlations. The results are plots are plotted in Fig. 5c.

Conditions: particles of 0.2 mm diameter, potential vs NHE, site density: $2\,nm^{-2}$.

Table 8

Transition point E'° and log K_d's (mL g^{-1}) for U(VI) and U(IV) sorption on tridentate carboxylic groups varying the carbonate concentration at pH 8.

Carbonate Conc. (M)	U (VI) Log K$_d$	U (IV) Log K$_d$	U (IV)/U (VI) E$'^\circ$ (V)
0.0010ˆ+0X	+ 14	+ 14	-0.62
2.20E-06	+ 14	+ 14	-0.65
2.20E-05	+ 11	+ 14	-0.67
2.20E-04	+ 8.7	+ 13	-0.70
2.20E-03	+ 5.7	+ 10	-0.71
2.20E-02	+ 2.7	+ 6.8	-0.72
2.20E-01	-0.3	+ 3.0	-0.70
2.20E+00	-3.3	-1.0	-0.69

Solid lines: in the water redox stability domain,

Dashed line: outside the water redox stability domain.

Total carbonate concentration: 0, 2.2×10^{-6}, 2.2×10^{-5}, 2.2×10^{-4}, 2.2×10^{-3}, 2.2×10^{-2}, 2.2×10^{-1} and 2.2×10^{-0} M from above to below.

For concentrations below 2×10^{-6} M, the Log K_d is found at ∼9.4 for U(VI). As the carbonate concentration rises, it increasingly interferes with the binding, reducing the K_d.

Each order of magnitude increase in carbonate concentration decreases the Log K_d by ∼3.

For the U(IV)/U(VI) couple the apparent redox potential, E′°, is found around −0.62 V, but its value varies: the most negative point (−0.72 V) being found for a carbonate concentration of 2.2×10^{-2} M. This is due to the presence of the U(VI) carbonato complexes. At higher carbonate concentrations U(IV) starts to form complexes, increasing the apparent standard redox potential of the couple. Again, all the redox domains where U(IV) forms are below the stability limits of water i.e. − 0.48 V. (Table 8).

5. Discussion

5.1. Effect of pH, E and dentate state on Kd in carbonate free solution

As the simplest case, the carbonate free systems exhibited the clearest trends (Fig. 3). The dominating factor under moderate to high pH was the transition between conditions where U(IV) prevails, and those where U(VI) species are dominant. As expected, the U(IV) is generally more sorbing than U(VI), likely due to the stereochemistry effects, stronger hydrolysis of U(IV) than U(VI) or both. An increase in pH mitigated however this effect. This is manifested by an increasing negative apparent redox potential E′°. Below pH 4, the possibility of U(III) became significant at low redox potentials, allowing the return to liquid phase mitigating consequently the Kd.

Between the three forms considered (mono-, bi- and tri-), monodentate is markedly different than the multi-dentate forms. In monoform, the decreasing pH slightly raises the Log Kd, while an opposite trend is true for the bi- and tri- forms. In addition, increasing pH has an increasing effect on tri-dentate than on bi-dentate. This would be consistent with more sites being available, leading to an increased probability of binding in these higher dentate states. However, both are similar at pH 6–8 range, which exhibits values that are consistent with real world measurements in natural environments. At low pH, both are reduced, but the effect is more marked in tridentate systems. It is presumably to be due to the slopes in the correlations e.g. data quality see Fig. 1 and Fig. 2a,b,c. This model is applicable to other redox sensitive elements.

5.2. Effect of pH, E and dentate state on Kd in carbonated solution

In presence of carbonate ligands, the competition effects between the carbonates complexes formation and the sorption by surface complexation are noticeable (See Fig.s 4 and 5). The dominating factor under moderate to high pH is still the hydrolysis (see the correlations), but this is herein between conditions where U(V) is locally/occasionally found, and those where U(VI) and U(IV) are dominant. The effect of this transition is significantly different, reducing the degree of step difference between the U(V) form and both U(VI) and U(IV) forms.

As expected, the U(IV) is more sorbing, likely due to the stereochemistry effects or actually due to a stronger hydrolysis of U(IV) than U(VI). An increasing pH mitigates this effect however, which is probably due to build-up of U(IV) and U(VI) hydroxo complexes, reducing the sorption of U. These effects also shift negatively the redox point of transition in the Log Kd - E plot. Below pH 4, the possibility of U(III) is becoming significant at low redox potentials.
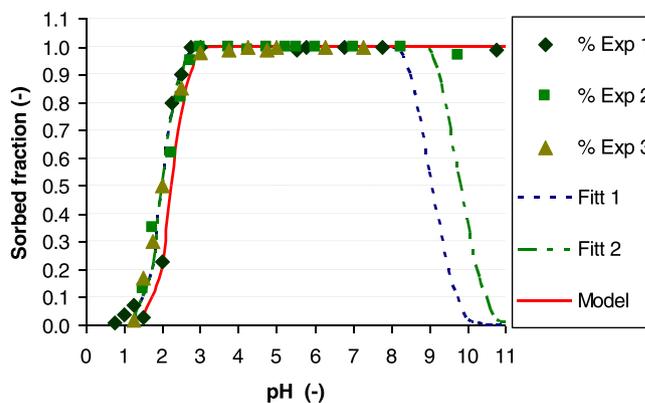

Fig. 6. Sorption curve of uranium(VI) on Amberlite CG-50 (weak carboxylic resin) from NaNO₃ solutions.

5.3. Testing the model calculation with the literature data

To test the results obtained by applying the sorption model developed in this study, one would use results gained for the sorption of uranium onto carboxylic coated latex (or model) colloids. If the carboxylic coated latex colloids exist and have been used for environmental studies, they were unfortunately not studied in great detail for the uranium sorption on these colloids.

The only study to authors' knowledge is reported by Pesavento et al. [52] who investigated the sorption of uranium(VI) on two cationic resins, containing different complexing groups, the iminodiacetic resin Chelex 100 and the weak carboxylic resin Amberlite CG-50. The sorption mechanism of the metal on the complexing resins was studied without and with addition of a competitive soluble ligand (L) that shifted, as expected, the sorption curves to higher pH values. The ligand competes with the resin for the complexation with the metal ion. Uranium is strongly sorbed on Amberlite CG-50 and involves the formation of the complex ML₂, in more acidic solution, with Log (120i) = −3.16. In the presence of the EDTA (Ethylenediaminetetraacetic acid) ligand, the complex ML₂(OH)₂ was characterized with Log (122i) = −5.15. In all the experiments the hydrolysis reaction in the aqueous phase was quantitatively considered. The sorption curve of uranium (VI) on Amberlite CG-50 (weak carboxylic resin) is reported on Fig. 6. The continuous line was calculated by considering the complexes ML₂ and ML₂(OH)₂. Note that above pH 9, the modelled sorption curve vs pH decreases which diverges with the experimental reality (100% sorbed above pH 9). The model developed in this study fits with the reality, the sorbed uranium fraction estimated remains 1.0 (100% sorption), reflecting that the model is more realistic that the model used by Pesavento et al. [52] because calculations herein take into account the formation of ternary surface complexes. More recently, Sun et al. [53] restated this ambiguous in their graphical abstract: after the edge around pH 4 under increasing pH the sorption is 100% from pH 6–9. Above pH 9 the ambiguous situation obliges the author to obscure the data above pH 9.

Conditions: data from Pesavento et al. [52].

(■) [NaNO₃] = 0.1 mol L⁻¹, V = 30 mL, c_M = 3.58×10^{-4} mol L⁻¹ and 0.1134 g of dry resin.

(◆) [NaNO₃] = 1.0 mol L⁻¹, V = 30 mL, c_M = 3.50×10^{-4} mol L⁻¹ and 0.1154 g of dry resin.

(▲)(- - - -) [NaNO₃] = 0.1 M, V = 31 mL, c_M = 2.79×10^{-7} mol L⁻¹ and 0.0983 g of dry resin.

The *dashed line* ─ ─ ─ and *dashed-and-dotted line* ── Red line are calculated with the intrinsic complexation constant of the complex mL₂ in 1.0 and 0.1 mol L⁻¹ NaNO₃, respectively.

data from this study.

—0, —2.2x10^{-6}, —2.2x10^{-5}, —2.2x10^{-4}, —2.2x10^{-3}, —2.2x10^{-2}, —2.2x10^{-1}, —2.2x10^{-0} M

Ref. Sun et al. (2021) [52].

Earlier, Van Loon & Kopajtic [54,55] presented their data on radionuclide adsorption on bitumen for strontium and nickel on an experimental basis and extended the data to americium and uranyl on a theoretical basis. In these studies they assumed that the surface of the bitumen particles is covered by carboxylic groups. Since their work was carried out in low ionic strength solution (10^{-3}), the ionic exchange was taken into consideration together with surface complexation. The bitumen particles are broadly dispersed 0.1–30 m, however, even if their study reported the effects of pH on sorption and models the adsorption on the carbonyl groups, at the surface, any attempt of comparison with the results reported in this study is difficult because of the differing units used for the sorption data (cm or L g^{-1}, respectively).

Zhang et al. [56], reported data on the adsorption and desorption of uranium(VI) onto humic acids derived from uranium-enriched lignite in fixed batch experiments. The results showed that the optimum pH level at which all the humic acids adsorbed uranium(VI) ranged from 5 to 8. The high uranium content of the humic acids was released into the solution at the pH values between 1 and 3. The uranium present in the humic acids may not affect the adsorption capacity of the uranium(VI), but the carboxylic groups in the humic acids play a significant role in controlling the adsorption capacity.

Bampaiti, et al. [57] investigated the biosorption of uranium from aqueous solutions by *Dictyopteris polypodioides* brown algae. The effects of pH, uranium concentration, mass of the adsorbent, temperature and contact time on the removal efficiency were studied and the results were simulated by various isotherm models. This study concluded that sorption process could be described as a combination of several mechanisms, including physical sorption, ion exchange and complexation, which would be expected from prior works, like Nakajima et al. [20] and Senko et al. [21].

In seawater conditions the sorption on particles (inorganic, organic and bioorganic) has been investigated by Li [58]. In these conditions, at pH 8 and in oxidising conditions Log K$_d$ was found to be around 4 for U (VI) and 8 for Th(IV), an analogous of U(IV), both in carbonated water (2×10^{-3} M). These values fits with the data calculated for U(VI) and U (IV), using the mono-dentate model developed in this study.

More recently, McGowan et al. [15] investigated the sorption of uranium from seawater on biomass material particles of 2 mm in size. They observed a very strong sorption of uranium on these materials that was justified by the specific structure of the uranyl complexes as reported by Lucks et al. [59]. Data are reported in Table 9.

The quantification of the uranium sorption data in the terms described by the model is usually difficult, as authors frequently use differing basis, such as providing them as fraction of U(VI) sorbed in %. Americium data may be reported instead of uranyl data because they may be more accurate and not really redox sensitive. Americium(III) has been considered as an analogue of uranyl by some groups e.g., Deneke [60]. This was previously addressed in the study of americium on marl colloids (organic coated clay) reported by Degueldre et al. [41].

Table 9 summarises the data obtained around pH 8 for montmorillonite, illite and chlorite (all natural and organic coated) as well as corundum (crystalline), for comparison. It seems that the concentration of bicarbonate displayed a relatively insignificant effect (under 2×10^{-2} M) on americium sorption onto clay-like particles, while their size has a direct effect on the sorption coefficient (see Eq. 23).

Since groundwater colloids are submicron particles, their sorption coefficient is consequently larger than the coefficients measured for these microscopic particles. Modelling of the sorption properties was carried out earlier using a surface complexation model extended to ternary surface complexes (e.g. Degueldre et al., [40]; Van Cappellen

Table 9

Comparison of experimental K$_d$ data or actinides (An) with data obtained using the surface complexation model. Am data summarised from Degueldre et al. (2001) . In Bold, experimental data for U.

K$_d$ (mL g^{-1})	pH (-)	[HCO$_3$] (M)	[An] (M)	d (m)	C$_{col}$ (ppm)	Colloids	Ref.
Inorganics							
1–5 × 10^6	8.6	2 × 10^2	3 × 10^{-11}	~0.05–5	1.7	Marl water	Degueldre et al.[41]
1–5 × 10^5	8.0	10^2	8 × 10^{-10}	~0.1–1	1–300	Illite	Degueldre et al.[40]
1–3 × 10^5	8.5	0	3 × 10^{-9}	n.r.	1 × 10^4	Illite	Gorgeon[63]
3–7 × 10^4	8.5	3 × 10^2	2 × 10^{-9}	n.r.	n.r.	Illite	Mucciardi et al.[64]
0.1–1 × 10^5	8.5	0	10^{-8}	5–50	5 × 10^3	Kao/Smec	Dolo[65]
1–3 × 104	8.0	1–3 × 10^{-3}	2 × 10^{-9}	44–63	7–12 × 10^{-3}	Clay	Beall & Allard[66]
0.5–2 × 10^4	8.0	0	3 × 10^{-7}	90–125	10^4	Corundum	Dozol &Hagemann[67])
1 × 10^5	8.0	0–10^2		~0.1–1	1–300	Illite	Degueldre et al.[40]
Bio-Organics							
3 × 10^3	**8.0**	**2 × 10^{-3}**	**1.5 × 10^{-8} U**	**~2000**	**~2000**	**Orange skin**	**McGowan et al.[16]**
4 × 10^3	**8.0**	**2 × 10^{-3}**	**1.5 × 10^{-8} U**	**~2000**	**~2000**	**Garlic diced**	**McGowan et al.[16]**
2 × 10^3	**8.0**	**2 × 10^{-3}**	**1.5 × 10^{-8} U**	**~2000**	**~2000**	**potato skin**	**McGowan et al.[16]**
1 × 10^4	**8.0**	**2 × 10^{-3}**	**1.0 × 10^{-8} U**	**200**	**~2000**	**natural**	**Li[58]**
1 × 10^9	**8.0**	**2 × 10^{-3}**	**2.0 × 10^{-12} Th**	**200**	**~2000**	**natural**	**Li[58]**
1 × 10^5	6.0	≈ 10^{-3}	10^{-8} Th	200		humic	Szabo et al.[53]
Model							
9 × 10^1 *	6.0	0	U(IV)*	200	30 × 10^3	Mono dentate	This work
1 × 10^2 *	8.0	0	U(IV)*	200	30 × 10^3	Mono dentate	This work
3 × 10^1	6.0	0	U(VI)	200	30 × 10^3	Mono dentate	This work
5 × 10^2	8.0	0$^-$	U(VI)	200	30 × 10^3	Mono dentate	This work
1 × 10^{-4} *	6.0	2 × 10^{-3}	U(IV)*	200	30 × 10^3	Bi dentate	This work
5 × 10^5 *	8.0	2 × 10^{-3}	U(IV)*	200	30 × 10^3	Bi dentate	This work (seawater)
1 × 10^{-6}	6.0	2 × 10^{-3}	U(VI)	200	30 × 10^3	Bi dentate	This work
1 × 10^0	8.0	2 × 10^{-3}	U(VI)	200	30 × 10^3	**Bi** dentate	This work (seawater)
1 × 10^5	8.0	2 × 10^{-3}	U(VI)	200	30 × 10^3	**Tri** dentate	This work (seawater)

Kao/Smec kaolinite/smectite mixed layer; n.r.: not reported, * reduction needed on > SuOH.

et al. [61]). In this work, the authors found a relationship between the sorption coefficient and the complexation of Am in solution, the site density at the colloid surface and the colloid size. It was concluded that the presence of free ion, hydroxo, carbonato or mixed complexes allows sorption when the Am tricarbonato complex is not yet formed. Only when the tricarbonato species, such as $[Am(CO_3)_3]^{3-}$, dominate, i.e. for a total carbonate concentration larger than 2×10^2 M, does sorption start to decrease significantly. A similar behaviour is observed for uranium(VI).

Calculations for spherical colloids of 200 nm size and density 2 g cm^3 yield Log K$_d$ values of 5 (with K$_d$ in mL g^{-1}) for $> Su$OH (with $Su =$ Al or Fe) sites with a density of 3 nm^2. For colloid sizes of 2000 and 20 nm, the Log K$_d$ values are, respectively, 4 and 6 (with K$_d$ in mL g^{-1}). The measured values (for the marl colloids of 50–5000 nm) are slightly larger because of the fractal aspect of the particles which present twinning's and sub-microscopic features increases the specific active surface.

Investigation of surface complexation of thorium by humic acid was carried out by Szabo et al. [62] using chemically immobilized humic acid on silica gel. Thorium(IV) may be considered as an analogue of uranium(IV). Here the silica material (20 m) is first loaded with humic acid. While the Th(IV) sorption isotherm is of a Freundlich type, it is possible to evaluate K$_d$'s of 2×104 mL g^{-1} at pH 4 and 4×104 mL g^{-1} at pH 6 for a total concentration of Th in solution of 1×10^{-8} mol L^{-1}. In these conditions (nonlinear isotherm), the K$_d$ data at pH 6 for a Langmuir isotherm (K$_{dL}$) could be estimated for K$_{dL}$ $= \lim_{c \to 0} K_{dF} \approx 1 \times 105$ mL g^{-1}.

At pH 8, the model K$_d$ values (see Table 9) calculated in this study are compared with other data, e.g. the data produced by Li [56]: namely 3×10^4 and 1×10^4 mL g^{-1} for U(VI) as well as 8×10^8 and 1×10^9 mL g^{-1} for U(IV) and Th(IV) respectively. Since the carbonates decrease strongly the sorption of U(VI) to be efficient the surface complexation in marine environment must include also bi- and tridentate species.

6. Conclusion

A model that evaluates for a given pH the sorption coefficient with the redox potential was developed for prediction of effects of the redox potential on the sorption of uranium onto models of bio-organic substrates. The model includes surface complexation on surface active sites (mono- or multi-dentate carboxyl groups) and complexation with ligands (carbonate) in the aqueous phase, and was applied to seawater. The effects of organics were discussed, considering the antagonist properties of carbonates. The calculations also considered effects of the redox potential for all the species formation at the surface and in solution. The model was applied to uranium, as an important redox sensitive element. The values of calculated sorption coefficient confirmed that the redox potential may affect the sorption of U, mostly U(VI), however its reduction to U(IV) at the sorbing substrates appears at the edge of the redox stability domain.

The calculated Log K$_d$ values were in relative agreement with scare experimental values reported in the literature.

The sorption analysis so far provides good predictive values for a limited subset of the experimental data, allowing reasonable prediction by modelling of the partition coefficients for a variety of water and biomass sorbents. Such data may help understand the formation of ore deposits (U(VI) = > U(IV)) and contribute to search for a versatile U extraction protocol from seawater. This last task could require to expand even more the variety of absorption substrates. A second paper on the sorption of uranium on polyphenolic model particles will be reported soon.

References

[1] R.C. Ewing, Environmental impact of the nuclear fuel cycle, Geological Society 236 Special Publications, London, 2004, pp. 7–23, https://doi.org/10.1134/S0016702916130115

[2] C. Degueldre, Uranium as a renewable for nuclear energy, Prog. Nucl. Energy 94 (2016) 17022, https://doi.org/10.1016/j.pnucene.2016.03.031

[3] C. Tsouris, uranium extraction, fuel from seawater, Nat. Energy 2 (2017) 174–186, https://doi.org/10.1038/nenergy.2017.22

[4] R. Djogic, M. Branica, Uranyl mixed-ligand complex formation in artificial seawater, Chem. Speciat. Bioavailab. 5 (1993) 101–105.

[5] A. Zhang, G. Uchiyama, T. Asakura, pH Effect on the uranium adsorption from seawater by a macroporous fibrous polymeric material containing amidoxime chelating functional group, React. Funct. Polym. 63 (2005) 143–153, https://doi.org/10.1016/j.reactfunctpolym.2005.02.015

[6] K. Sekiguchi, K. Saito, S. Konishi, S. Furusaki, T. Sugo, H. Nobukawa, Effect of seawater temperature on uranium recovery from seawater using amidoxime adsorbents, Ind. Eng. Chem. Res. 33 (1994) 662–666, https://doi.org/10.1021/ie00027a025

[7] T. Aihara, A. Goto, T. Kago, K. Kusakabe, S. Morooka, Rate of adsorption of uranium from seawater with a calix(6)arene adsorbent, Sep. Sci. Technol. 27 (1992) 1655–1667, https://doi.org/10.1080/01496399208029230

[8] H. Yamashita, Y. Ozawa, F. Nakajima, T. Murata, The collection of uranium from seawater with hydrous metal oxide. III. The effects of diverse ions in seawater on uranium adsorption by hydrous titanium(IV) oxide, Bull. Chem. Soc. Jpn. 53 (1980) 1331–1334, https://doi.org/10.1246/bcsj.53.1331

[9] T. Sugo, M. Tamada, T. Seguchi, T. Shimizu, M. Uotani, R. Kashima, Recovery system for uranium from seawater with fibrous adsorbent and its preliminary cost estimation, J. -STAGE 43 (2001) 1010–1016, https://doi.org/10.3327/jaesj.43.1010

[10] E. Schneider, D. Sachde, The cost of recovering uranium from seawater by a braided polymer adsorbent system, Sci. Glob. Secur. 21 (2013) 134–163, https://doi.org/10.1080/08929882.2013.798993

[11] NEA and IAEA, Uranium 2016 – resource, production and demand, OECD publishing, 2016, p. 548.

[12] N. Gaur, G. Flora, M. Yadava, A. Tiwaria, A review with recent advancements on bioremediation-based abolition of heavy metals, Environ. Sci. Process. Impacts 16 (2014) (2014) 180–193, https://doi.org/10.1039/C3EM00491K

[13] A. Nakajima, T. Sakaguchi, Adsorption of uranium by vegetable crude drugs, Agric. Biol. Chem. 53 (1989) 2853–2859, https://doi.org/10.1080/00021369.1989.10869765

[14] Aly, Z., Luca, V., Uranium extraction from aqueous solution using dried pyrolyzed tea and coffee wastes, J Radioanal. Nucl. Chem, 295, 889–900. https://doi.org/10.1007/s10967–012-1851–6.

[15] P.D. Pathak, S.A. Mandavgane, B.D. Kulkarni, Fruit peel waste as a novel low-cost bio adsorbent, Rev. Chem. Eng. 31 (2013) (2015) 361–381, https://doi.org/10.1515/revce-2014-0041

[16] S. McGowan, H. Zhang, C. Degueldre, Testing sorption of uranium from seawater on waste biomass: a feasibility study, Fuel 315 (2022) 123224, , https://doi.org/10.1016/j.fuel.2022.123224

[17] I. Dakova, I.B. Karadjova, V.T. Georgieva, G.S. Georgiev, Polycarboxylic microsphere polymer gel for solid phase extraction of trace elements, Microchim. Acta 164 (2009) 55–61, https://doi.org/10.1007/s00604-008-0031-4

[18] S. Vaz Jr., Chapt. 1.2: Plant Biomass Diversity and Composition. Pg. 5, Analytical Techniques and Methods for Biomass, Springer, 2016, , https://doi.org/10.1007/978-3-319-41414-0

[19] I. Langmuir, The adsorption of gases on plane surfaces of glass, mica and platinum, J. Am. Chem. Soc. 49 (1918) 1361–1403, https://doi.org/10.1021/ja02242a004

[20] H. Freundlich, Über die Adsorption in Lösungen, Z. für Phys. Chem. 57 (1907) 385–470, https://doi.org/10.1515/zpch-1907-5723

[21] Ch Sheindorf, M. Rebhun, M. Sheintuch, A Freundlich-type multicomponent isotherm j coll interf Sci, 79 (1981) 136–142, https://doi.org/10.1016/0021-9797(81)90056-4

[22] I. McKinley, A. Scholtis, A comparison of radionuclide sorption data base in recent performance assessments, J. Contam. Hydrol. 13 (1993) 347–363, https://doi.org/10.1016/0169-7722(93)90070-9

[23] Gr.J. Millar, J.G. Outram, Ch.W. Leung, Methodology of isotherm generation: Multicomponent K+ and H+ ion exchange with strong acid cation resin, Sep. Purif. Technol. 251 (2020) 117360, , https://doi.org/10.1016/j.seppur.2020.117360

[24] Gr.J. Millar, G.L. Miller, Sh Papworth, , Factors influencing kinetic and equilibrium behaviour of sodium ion exchange with strong acid cation resin, Sep. Purif. Technol. 251 (2020) 11736, https://doi.org/10.1016/j.seppur.2020.117360

[25] A. Wissocq, C. Beaucaire, Ch Latrille, Application of the multi-site ion exchange model to the sorption of Sr and Cs on natural clayey sandstone, Appl. Geochem. 93 (2018) 167–177, https://doi.org/10.1016/j.apgeochem.2017.12.010

[26] E. Reinoso-Maset, J. Ly, Study of uranium(VI) and radium(II) sorption at trace level on kaolinite using a multisite ion exchange model, J. Environ. Radioact. 157 (2016) 136–148, https://doi.org/10.1016/j.jenvrad.2016.03.014

[27] N. Esfandiar, R. Suri, E.R. McKenzie, Competitive sorption of Cd, Cr, Cu, Ni, Pb and Zn from stormwater runoff by five low-cost sorbents; Effects of co-contaminants, humic acid, salinity and pH, J. Hazard. Mater. A 423 (2022) 126938, https://doi.org/10.1016/j.jhazmat.2021.126938

[28] Wenwen Cai, Divina A. Navarro, Rai S. Kookana, Increasing ionic strength and valency of cations enhance sorption through hydrophobic interactions of PFAS with soil surfaces, Sci. Total Environ. 817 (2022) 152975, , https://doi.org/10.1016/j.scitotenv.2022.152975

[29] H. Mei, N. Aoyagi, Y. Tachi, Uranium (VI) sorption on illite under varying carbonate concentrations: batch experiments, modeling, and cryogenic time-resolved laser fluorescence spectroscopy study, Appl. Geochem. 136 (2022) 105178, , https://doi.org/10.1016/j.apgeochem.2021.105178

[30] K. Burdzy, A. Aurich, D. Kołodyńska, Green citric acid in the sorption process of rare earth elements, Chem. Eng. J. 437 (2022) 135366, https://doi.org/10.1016/j.cej.2022.135366

[31] U. Alonso, C. Degueldre, Modelling americium sorption onto colloids: effect of redox potential, Colloids Surf. A: Physicochem. Eng. Asp. 217 (2003) 55–62, https://doi.org/10.1016/S0927-7757(02)00558-7

[32] C. Degueldre, A. Kline, Study of thorium association and surface precipitation on colloids, Earth Planet. Sci. Lett. 264 (2007) 104–113, https://doi.org/10.1016/j.epsl.2007.09.012

[33] J.T. Padilla, H. Magdi Selim, A.L. Gaston, Modelling the competitive sorption and transport of Ni(II) and Zn(II) in soils: Comparing two multi-component approaches (Available online), J. Contam. Hydrol. 15 (2022) 104108, , https://doi.org/10.1016/j.jconhyd.2022.104108

[34] T. Missana, U. Alonso, M. García-Gutiérrez, Evaluation of component additive modelling approach for europium adsorption on 2:1 clays: experimental, thermodynamic databases, and models, Chemosphere 272 (2021) 129877, , https://doi.org/10.1016/j.chemosphere.2021.129877

[35] D. Lovley, E. Phillips, Y. Gorby, E.R. Landa, Microbial reduction of uranium, Nature 350 (1991) 413–416, https://doi.org/10.1038/350413a0

[36] J.M. Senko, J.D. Istok, J.M. Suflita, L.R. Krumholzan, In-Situ evidence for uranium immobilization and remobilization, Environ. Sci. Technol. 36 (2002) 1491–1496, https://doi.org/10.1021/es011240x

[37] C.A. Degueldre, R.J. Dawson, V. Najdanovic-Visaka, Nuclear fuel cycle, with a liquid ore and fuel: toward renewable energy, Sustain. Energy Fuels 3 (2019) 1693–1700, https://doi.org/10.1039/C8SE00610E

[38] C. Degueldre, St McGowan, Simulating uranium sorption onto inorganic particles: The effect of redox potential, J. Environ. Radioact. 225 (2020) 106408, , https://doi.org/10.1016/j.jenvrad.2020.106408

[39] R.E. Jones, D.H. Templeton, The crystal structure of acetic acid, Acta Cryst. 11 (1958) 484–487, https://doi.org/10.1107/S0365110×58001341

[40] C. Degueldre, H.J. Ulrich, H. Silby, Sorption of 241Am on montmorillonite, illite and hematite colloids, Radiochim. Acta 65 (1994) 173–179, https://doi.org/10.1524/ract.1994.65.3.173

[41] C. Degueldre, A. Bilewicz, W.H. Hummel, J.L. Loizeau, Sorption behaviour of Am on marl groundwater colloids, J. Environ. Radioact. 55 (2001) 241–253, https://doi.org/10.1016/S0265-931X(00)00210-1

[42] R.F. Carbonaro, Y.B. Atalay, D.M. Di Toro, Linear free energy relationships for metal-ligand complexation: bidentate binding to negatively-charged oxygen donor atoms, Geochim Cosmochim. Acta 75 (2011) 2499–2511, https://doi.org/10.1016/j.gca.2011.02.027

[43] Th Loiseau, I. Mihalcea, N. Henry, Ch Volkringer, The crystal chemistry of uranium carboxylates, Coord. Chem. Rev., 266– 267 (2014) 69–109, https://doi.org/10.1016/j.ccr.2013.08.038

[44] NEA, Chemical thermodynamics of uranium, Data bank Radioactive waste management, (2004) OECD/NEA, 2004.

[45] I. Grenthe, J. Drozdzinsky, T. Fujino, E. Buck, T.E. Albrecht-Schmitt, S.F. Wolf, Uranium, The chemistry of the actinide and transactinide elements, Springer, 2006.

[46] A. Martell, R.M. Smith, Critical stability constants Vol 1–6 Springer-Verlag US, 1989.

[47] R.E. Jones, R.H. Templeton, The crystal structure of acetic acid, Acta Crystallogr. Volume 11 (Issue 7) (1958) 484–487, https://doi.org/10.1107/S0365110×58001341

[48] F.J. Millero, Chemical oceanography, CRC press, 2013.

[49] V.M.C. Rérolle, C.F.A. Floquet, M.C.M.C. Mowlem, D.P. Connelly, E.P. Achterberg, R.R.G.J. Bellerby, Seawater-pH measurements for ocean-acidification observations, TrAC Trends Anal. Chem. 40 (2012) 146–157, https://doi.org/10.1016/j.trac.2012.07.016

[50] V.M.C. Rérolle, C.F.A. Floquet, A.J.K. Harris, M.C. Mowlem, R.R.G.J. Bellerby, E.P. Achterberg, Development of a colorimetric microfluidic pH sensor for autonomous seawater measurements, Anal. Chim. Acta 786 (2013) 124–131, https://doi.org/10.1016/j.aca.2013.05.008

[51] J.D. Sharp, R.H. Byrne, X. Liu, R.A. Feely, E.E. Cuyler, R. Wanninkhof, S.R. Alin, Spectrophotometric determination of carbonate ion concentrations: elimination of instrument-dependent offsets and calculation of In Situ saturation states, Environ. Sci. Technol. 51 (2017) 9127–9136, https://doi.org/10.1021/acs.est.7b02266

[52] M. Pesavento, R. Biesuz, G. Alberti, M. Sturini, Characterization of the sorption of uranium(VI) on different complexing resins, Anal. Bioanal. Chem. 376 (2003) 1023–1029, https://doi.org/10.1007/s00216-003-1951-9

[53] Y. Sun, et al., Application of surface complexation modelling on adsorption of uranium at water-solid interface: a review, Environ. Pollut. 278 (2021) 116861, , https://doi.org/10.1016/j.envpol.2021

[54] L.R. Van Loon, Z. Z. Kopajtic, The adsorption of radionuclides on bitumen, Part I strontium, Radiochim. Acta 55 (1991) 83–89, https://doi.org/10.1524/ract.1991.55.2.83

[55] L.R. Van Loon, Z. Kopajtic, The adsorption of radionuclides on bitumen Part II nickel, Radiochim. Acta 55 (1991) 91–94, https://doi.org/10.1524/ract.1991.55.2.91

[56] Y. Zhang, Y. Li, Y. Ning, D. Liu, P. Tang, Z. Yang, Y. Lu, X. Wang, Adsorption and desorption of uranium(VI) onto humic acids derived from uranium-enriched lignites, Water Sci. Technol. 77 (2018) 920–930, https://doi.org/10.2166/wst.2017.608

[57] A. Bampaiti, S. S. Yusan, S. Aytas, E. Pavlidou, F. Noli, Investigation of uranium biosorption from aqueous solutions by Dictyopteris polypodioides brown algae, J. Radioanal. Nucl. Chem. 307 (2016) 1335–1343, https://doi.org/10.1007/s10967-015-4289-9

[58] Y.H. Li, Ultimate removal mechanisms of elements from the ocean, Geochim. Cosmochim. Acta 45 (1981) 1659–1664, https://doi.org/10.1016/0016-7037(81)90001-6

[59] C. Lucks, A. Rossberg, S. Tsushima, H. Foerstendorf, A.C. Scheinost, G. Bernhard, Aqueous uranium(VI) complexes with acetic and succinic acid: speciation and structure revisited, Inorg. Chem. 51 (2012) 12288–12300, https://doi.org/10.1021/ic301565p

[60] M. Deneke, Personal communication (2010).

[61] P. Van Cappellen, L. Charlet, W. Stumm, P. Wersin, A surface complexation model of the carbonate mineral–aqueous solution interface, Geochim. Cosmochim. Acta 57 (1993) 3505–3518, https://doi.org/10.1016/0016-7037(93)90135-J

[62] G. Szabo, J. Guczi, P.E. Reiller, H. Geckeis, R.A. Bullman, Investigation of complexation of thorium by humic acid using chemically immobilized humic acid on silica gel, Radiochim. Acta 94 (2006) 553–557, https://doi.org/10.1524/ract.2006.94.9.553

[63] Gorgeon, L., 1994. Contribution à la modélisation physico-chimique de la rétention de radioéléments à vie longue par des matériaux argileux. Unpublished Doctoral Thesis, Université de Paris 6.

[64] Mucciardi, A., Booker I., Orr E., Cleveland D., 1978, Statistical investigation of the mechanics controlling radionuclide sorption. WISAP Task 4. Second contractor meeting proceedings, PNL-SA7352.

[65] Dolo, J.M., 1991. Etude de la rétention de l'américium trivalent, du neptunium pentavalent, et de l'uranium hexavalent par un matériau argileux. Unpublished Doctoral, Thesis, Thèse Conservatoire National des Arts et Métiers, Paris.

[66] G. Beall, B. Allard, Sorption of actinides from aqueous solution under environmental conditions, in: P. Tewari (Ed.), Adsorption from aqueous solutions, vol. 193, Plenum Press, New York, 1981.

[67] M. Dozol, R. Hagemann, D.C. Hoffman, J.P. Adloff, H.R. von Gunten, J. Foos, K.S. Kasprzak, Y.F. Liu, I. Zvara, H.J. Ache, H.A. Das, R.J.C. Hagemann, G. Herrmann, P. Karol, W. Maenhaut, H. Nakahara, M. Sakanoue, J.A. Tetlow, G.B. Baro, J.J. Fardy, P. Benes, K. Roessler, E. Roth, K. Burger, E. Steinnes, J.M. Konstanski, M. Peisach, J.O.L. Hinzin, N.K. Aras, B.F. Myasoedov, N.E. Holden, Radionuclide migration in groundwaters: Review of the behavior of actinides, Pure Appl. Chem. 65 (1993) 1081–1102.